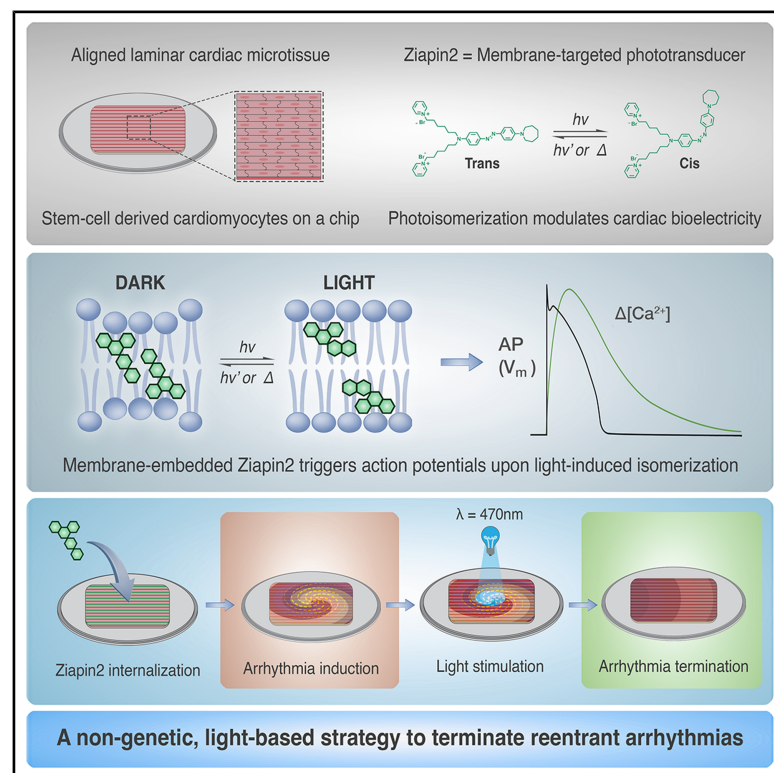


Optotermination of spiral wave reentry by a membrane-targeted phototransducer

Graphical abstract



Authors

Chiara Florindi, Kevin Shani, Vito Vurro, ..., Antonio Zaza, Kevin Kit Parker, Francesco Lodola

Correspondence

francesco.lodola@unimib.it

In brief

Cardiac arrhythmias arise from abnormalities in the generation or propagation of electrical impulses in the heart and remain challenging to treat with current therapies. Here, we test *in vitro* whether Ziapi2, a membrane-targeting molecular photoswitch previously shown to modulate cardiac excitability, can terminate reentrant arrhythmias. In engineered stem-cell-derived human cardiac microtissues, Ziapi2 photoisomerization effectively disrupts spiral waves and abolishes reentry. These findings highlight small-molecule photoswitches as a potential strategy for precise optical control of cardiac bioelectricity.

Highlights

- Ziapi2 is a molecular photoswitch that enables optical control of cardiac bioelectricity
- Engineered hiPSC cardiac microtissues represent a model of spiral wave reentrant arrhythmias
- Ziapi2 photoisomerization disrupts and terminates spiral wave reentry

Article

Optotermination of spiral wave reentry by a membrane-targeted phototransducer

Chiara Florindi,^{1,2,3} Kevin Shani,^{3,4} Vito Vurro,^{2,3} Yongjun Jang,^{3,4} Paola Moretti,^{2,5} Maksymilian Prondzynski,^{4,6} Yashasvi Tharani,⁴ Vassilios J. Bezzerides,⁴ William T. Pu,^{4,7} Chiara Bertarelli,^{2,5} Guglielmo Lanzani,^{2,8} Antonio Zaza,¹ Kevin Kit Parker,^{3,4,7} and Francesco Lodola^{1,2,9,*}

¹Department of Biotechnology and Biosciences, University of Milano-Bicocca, 20126 Milan, Italy

²Center for Nano Science and Technology, Istituto Italiano di Tecnologia, 20134 Milan, Italy

³Disease Biophysics Group, John A. Paulson School of Engineering and Applied Science, Harvard University, Boston, MA 02134, USA

⁴Department of Cardiology, Boston Children's Hospital, Boston, MA 02115, USA

⁵Department of Chemistry, Materials and Chemical Engineering "Giulio Natta", Politecnico di Milano, 20133 Milan, Italy

⁶Harvard Medical School, Harvard University, Boston, MA 02115, USA

⁷Harvard Stem Cell Institute, Harvard University, Cambridge, MA 02138, USA

⁸Department of Physics, Politecnico di Milano, 20133 Milan, Italy

⁹Lead contact

*Correspondence: francesco.lodola@unimib.it

<https://doi.org/10.1016/j.celbio.2026.100453>

THE BIGGER PICTURE Arrhythmias pose significant challenges in clinical cardiac care, with current treatments often carrying risks of complications and recurrence. Strategies capable of controlling cardiac bioelectricity with greater spatial precision and reduced invasiveness could open up new therapeutic opportunities. Ziapin2 is an amphiphilic, photochromic molecule previously shown to modulate cardiomyocyte excitability upon light stimulation. Here, we test whether Ziapin2-mediated photostimulation can interrupt reentrant arrhythmias. Using engineered, aligned cardiac microtissues derived from wild-type and diseased human-induced pluripotent stem cell cardiomyocytes, we first establish stable reentrant spiral waves and then show that light stimulation in the presence of Ziapin2 disrupts these dynamics and terminates reentry. These findings provide proof of principle for non-genetic optical control of arrhythmogenic dynamics and highlight the potential of small-molecule photoswitches to manipulate cardiac bioelectricity with high spatio-temporal precision.

SUMMARY

Optostimulation is rapidly emerging as a promising approach to control cardiac bioelectricity, combining minimal invasiveness with unparalleled spatiotemporal precision and reversibility. Building on previous findings demonstrating that Ziapin2, a membrane-targeted molecular photoswitch, can modulate cardiomyocyte electrophysiology upon visible light stimulation, we evaluated its potential to precisely terminate reentry-based arrhythmias. Reentrant activity was induced in aligned laminar cardiac microtissues from human-induced pluripotent stem-cell-derived cardiomyocytes (hiPSC-CMs), using an S1S2 electrical pacing protocol in wild-type tissues and rapid pacing combined with catecholamine exposure in gene-edited microtissues harboring the CPVT-associated S404R variant in the *RYR2* gene. Photostimulation disrupted spiral wave dynamics in Ziapin2-loaded tissues, whereas it had no effect on vehicle-treated controls. These results provide proof of principle for Ziapin2-mediated optotermination of arrhythmias and highlight its potential as a precise, non-genetic, and minimally invasive strategy for arrhythmia modulation.

INTRODUCTION

Sudden cardiac death is a major public health issue, accounting for 15%–20% of all deaths worldwide. Cardiovascular therapy has evolved significantly over the past 50 years; however, antiarrhythmic drugs remain limited by their proarrhythmic potential.

For example, the cardiac arrhythmia suppression trial (CAST) revealed that flecainide, a widely used class IC antiarrhythmic drug, increased mortality despite its efficacy in suppressing premature ventricular contractions.¹ Standard antiarrhythmic approaches often involve the ablation of arrhythmia substrates and the use of implantable cardioverter devices (ICDs) for

life-threatening arrhythmias. Implantable devices, such as pacemakers and ICDs, work by delivering controlled electrical impulses to restore or maintain a normal heart rhythm. In contrast, catheter-based ablation uses targeted energy delivery to destroy the abnormal tissue causing the arrhythmia. Despite their successes, these electrical therapies are limited due to issues such as non-specific activation of surrounding tissues, patient discomfort, finite device longevity, and potential for arrhythmia recurrence—complications that affect the patient's quality of life.^{2–4} This highlights the urgent need for more effective, less invasive therapies that target arrhythmias with greater precision and fewer side effects.

A potential strategy to address these challenges is to replace electricity with light as a stimulating tool. Optical stimulation is emerging as a promising alternative to traditional approaches for various research and therapeutic applications, offering several key advantages: minimal energy consumption, precise delivery to targeted tissues, and high spatial and temporal resolution.⁵ One notable method in this field is optogenetics, which involves the genetic modification of cells to express light-sensitive ion channels.^{6,7} This approach has shown significant success in terminating cardiac arrhythmias.^{8–15} However, several challenges, including stable and specific opsin expression and efficient gene delivery, remain to be addressed before broader clinical applicability can be achieved.¹⁶

As an emerging and complementary strategy, organic “small molecules” can be used to confer light sensitivity to excitable cells through covalent or non-covalent interactions with ion channels or the sarcolemma, providing a non-genetic, chemically tunable framework that expands the current landscape of optical cardiac modulation approaches.^{17–25} Recently, we synthesized Ziapin2, a light-responsive molecule with an aminoazobenzene core and an amphiphilic structure.^{26–28} The compound can integrate into cell membranes and change its conformation when exposed to visible light (470nm). This alteration affects the thickness of the cell membrane, leading to changes in membrane capacitance and, consequently altering the cell's membrane potential.^{26–28} When introduced into human-induced pluripotent stem-cell-derived cardiomyocytes (hiPSC-CMs) and adult mouse ventricular cardiomyocytes,^{29,30} Ziapin2 triggered action potentials in response to light-induced isomerization through the activation of stretch-activated channels.^{29,31} Of particular interest, when added to a cardiac microphysiological model that mimics the organization and mechanical properties of the heart, Ziapin2 enabled the control of the whole excitation-contraction process via light stimulation.³² These encouraging findings suggest that these light-sensitive compounds hold the potential for non-genetic, contactless, and temperature-independent regulation of cardiac bioelectricity, indicating their strong suitability for antiarrhythmic purposes.

In this study, we tested the hypothesis that Ziapin2 can effectively terminate reentry arrhythmias by using light stimulation to modulate cellular activity in a controlled manner. To assess this, we first generated stable reentry arrhythmias in aligned laminar cardiac microtissues, derived from both wild-type and gene-edited hiPSC-CMs carrying the S404R variant of the *RYR2* gene, a known pathogenic mutation associated with catecholaminergic polymorphic ventricular tachycardia (CPVT). By employing optical mapping of Ca^{2+} signals (as a reporter of excitation), we demon-

strate the ability of Ziapin2-mediated photostimulation to terminate reentrant activity in both wild-type and disease-mimicking microtissues, providing a functional basis for exploring optical control as a targeted strategy to interrupt arrhythmic circuits and advance minimally invasive approaches in cardiac therapy.

RESULTS AND DISCUSSION

Photostimulation efficacy of Ziapin2 in aligned laminar microtissues

To assess the functional photostimulation potential of Ziapin2, we tested its ability to trigger excitation in aligned laminar cardiac microtissues^{8,32,33} seeded with hiPSC-CMs generated in a bioreactor³⁴ by using optical mapping of intracellular Ca^{2+} signals as a readout of excitation and monitoring the generation and propagation of light-induced Ca^{2+} transients (Figure 1A). Microtissues were incubated with two concentrations of Ziapin2, 25 μM and 50 μM , followed by a 7-min washout to remove uninternalized molecules. Upon 470 nm point-light stimulation at 1 Hz, matching Ziapin2's absorption peak, we examined the initiation of Ca^{2+} wavefronts from the illumination site that propagate with a conduction velocity (CV) of 5.49 ± 0.14 cm/s. While 25 μM Ziapin2 showed minimal effect (data not shown), 50 μM was identified as the effective concentration for inducing a robust photoresponse (Figure 1B).

To confirm the safety of this approach, we assessed cell viability and oxidative stress under both dark and light-stimulated conditions. Cell viability and metabolic activity were evaluated using the AlamarBlue assay, comparing untreated, vehicle-treated, and Ziapin2-treated hiPSC-CMs. No significant differences were observed across conditions, suggesting that neither Ziapin2 internalization nor subsequent light exposure compromised cell health or function (Figure 1C).

To assess potential oxidative stress, we measured intracellular reactive oxygen species (ROS) levels using the CellROX assay. ROS levels remained comparable among all experimental groups, demonstrating that light activation of Ziapin2 does not induce oxidative damage (Figure 1D).

These data confirm the biocompatibility and photostability of Ziapin2 in our experimental settings.

Generation of a stable reentry circuit in the aligned laminar cardiac microtissue

To test the hypothesis that light-induced modulation of cardiac cell electrical potential through Ziapin2 isomerization may serve as an effective strategy for terminating arrhythmias, we investigated its effect on reentrant circuits, a primary mechanism underlying several types of cardiac arrhythmias. The formation of stable rotors requires that the tissue domain be sufficiently large to support a reentrant circuit. This condition is governed by the wavelength (WL) of the propagating electrical wavefront, defined as the following:

$$\text{WL} = \text{CV} \times \text{APD}$$

where CV is the conduction velocity, and APD is the action potential duration.

To achieve this, we considered the electrophysiological parameters of the hiPSC-CMs generated in the bioreactor, which

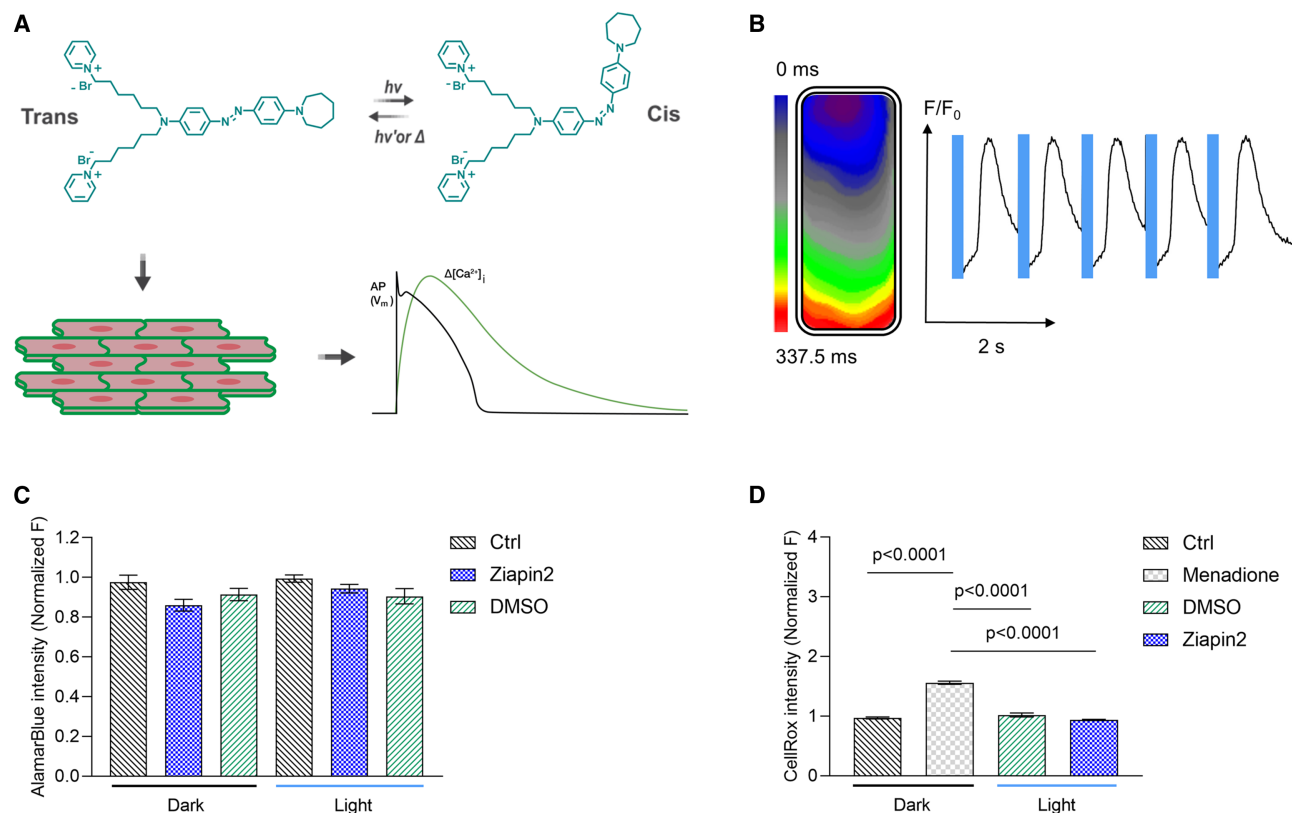


Figure 1. Ziapin2-mediated effects in hiPSC-CMs microtissues

(A) Visual representation of Ziapin2 molecules during internalization in aligned hiPSC-CMs and their light-induced *trans* → *cis* photoisomerization. Upon photostimulation, Ziapin2 modulates cardiac excitability, triggering electrical activity that propagates across the tissue.

(B) Representative isochrone map and traces of Ziapin2-mediated Ca²⁺ propagation in hiPSC-CMs microtissues triggered by 1Hz light stimulation.

(C) Effect of Ziapin2 internalization and light exposure on hiPSC-CM viability assessed by the Alamar Blue assay. Groups include untreated cells (Ctrl), molecule-loaded (Ziapin2), and vehicle-treated hiPSC-CMs (DMSO); $n = 32$ wells from 3 WT-Cas9 hiPSC-CMs differentiations. Statistical analysis was performed using the Kruskal-Wallis test.

(D) Effect of light stimulation on oxidative stress in hiPSC-CMs evaluated using the CellROX assay. Groups included untreated cells (Ctrl, $n = 237$, $N = 3$) and Menadione-treated cells ($n = 244$, $N = 3$) as positive control, both kept in the dark, as well as vehicle-treated hiPSC-CMs (DMSO, $n = 71$, $N = 3$) and Ziapin2-treated cells ($n = 178$, $N = 3$), which were subjected to 100-ms pulsed light stimulation. Where n = number of wells and N = number of WT-Cas9 hiPSC-CMs differentiations. Statistical analysis was performed using the Kruskal-Wallis test.

exhibited APD at 90% of repolarization (APD₉₀) between 200 and 400 ms³⁴ and a CV of approximately 5 cm/s. Based on this principle, we designed our engineered constructs by increasing their dimensions while maintaining the fabrication criteria previously reported³³ (i.e., laser-guided alignment, gelatin-based scaffolds, and hiPSC-CM seeding), as described here in the methods section and illustrated in Figure S1. Micromolded grooves guided the alignment of hiPSC-CMs, recapitulating the anisotropic architecture of native cardiac tissue. The resulting aligned laminar tissues measured 10 mm in length and 9 mm in width, thereby providing a spatial domain that is theoretically sufficient to support functional reentry and rotor stabilization (Figure 2A). The microtissues were characterized by highly anisotropic cellular alignment, as confirmed by confocal microscopy imaging (Figure 2B). Nuclei were stained with Hoechst, sarcomeric F-actin was labeled with FITC-conjugated antibodies, and cytoskeletal organization was visualized using Alexa-Fluor-647-conjugated phalloidin. Quantitative analysis of phalloidin-stained actin filament orientation relative

to the substrate grooves (0° indicating perfect alignment) showed a mean alignment angle of $\theta_{\text{mean}} = 4.85^\circ \pm 0.75^\circ$, evidencing a highly anisotropic tissue architecture conducive to organized electrical conduction (Figure 2C).

To generate stable reentrant activity within the aligned laminar cardiac microtissues, we employed an S1S2 electrical stimulation protocol, a well-established approach for inducing functional reentry in excitable media (Figure S2, see methods section for details). Reentry was considered successfully induced if the activation wavefront completed multiple full rotations and was defined as sustained if it persisted for at least 30 s.³⁵

Ziapin2 photostimulation terminates arrhythmias in WT aligned laminar microtissues

Following the induction of sustained reentry (duration > 30 s) with a mean cycle length (CL) of 0.57 ± 0.08 s, we next evaluated whether targeted light stimulation of Ziapin2-treated tissues could effectively terminate the arrhythmic activity. To this end,

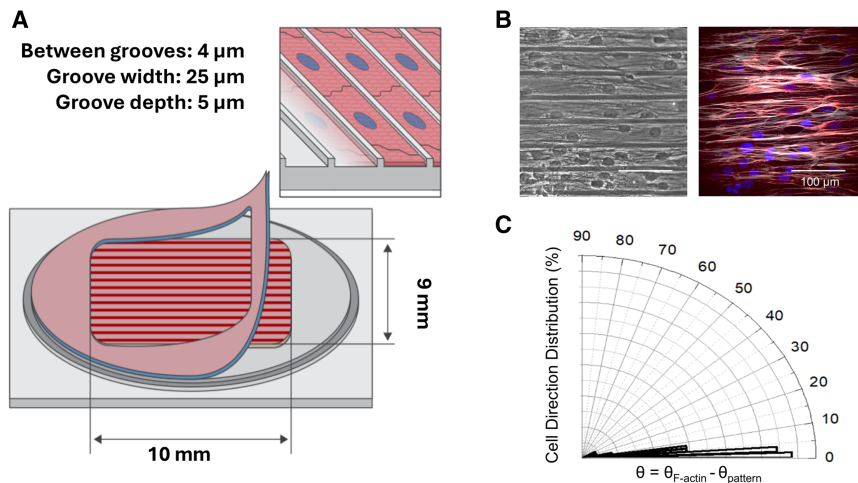


Figure 2. Characterization of aligned laminar cardiac microtissues and generation of a stable reentry circuit

(A) Schematic representation of the gelatin-based molded scaffold used to generate structurally organized cardiac microtissues. The figure illustrates the scaffold geometry and dimensions, optimized to promote cell alignment and laminar organization across the tissue construct.

(B) Representative confocal microscopy images of aligned laminar microtissues derived from hiPSC-CMs, stained with Hoechst (blue), FITC-conjugated anti-F-actinin (red), and Alexa-Fluor-647-conjugated phalloidin (white).

(C) Quantitative analysis of hiPSC-CMs orientation on cardiac microphysiological tissues. The orientation distribution is normalized to the pattern direction ($n = 48$ ROI, $N = 4$ tissues from 3 WT-Cas9 hiPSC-CMs differentiations).

an external LED source was positioned at the center of the microtissue, illuminating an area of approximately 0.78 mm^2 , thereby selectively targeting the core region of the reentrant circuit (Figure 3A). Light stimulation (17 mW/mm^2) was applied following a stepwise protocol, ranging from 100-ms single pulses to pulse trains at 0.5 and 1 Hz (see methods for details). Overall, the protocol successfully terminated spiral waves in 100% of Ziapin2-treated microtissues ($N = 6$, $p = 0.0022$, Fisher exact test, Figures 3B and 3D). Importantly, in all cases, the tissues remained excitable and could be reactivated by electrical field stimulation following optotermination (Figure S4). Notably, stimulation at 0.5 Hz showed a higher efficacy, terminating reentry in 4 out of 6 preparations (Figure 3C). Conversely, light stimulation failed to stop arrhythmias in platforms treated with the vehicle (DMSO), underscoring Ziapin2-specific efficacy in this context (Figure S3). These results suggest that, while repetitive pulsed stimulation increases success rates, single-pulse stimulation can terminate reentry in select cases and may represent a more energy-efficient and thermally conservative strategy, reducing the cumulative photonic and thermal burden on the tissue.

Light-induced termination of spiral waves in Ziapin2-loaded CPVT microtissues

To evaluate the impact of our treatment under conditions that closely mimic the disease state, we tested the efficacy of our approach in CPVT cultures, where reentry was likely induced by spontaneously triggered activity (no S1S2 stimulation required).³⁶ For this purpose, hiPSC-CMs carrying the patient-specific S404R variant in *RYR2* were seeded onto gelatin-grooved platforms, leading to aligned laminar cardiac microtissues (Figure 4A). Initially, we assessed the phenotype of these cells and observed spontaneous Ca^{2+} release events typical of the pathology (Figure S5A).³⁷ This finding confirmed the presence of aberrant Ca^{2+} handling as a source of ectopic activity. Leveraging the genetic background of these cells, we facilitated triggered activity by applying runs of high-frequency electrical stimulation combined with exposure to catecholamines. Specifically, the cultures were perfused with isoproterenol $1 \mu\text{M}$ and subjected to field stimulation at increasing frequencies (up to 2 Hz).⁸ Under these condi-

tions, reentrant circuits emerged spontaneously, as shown in Figure S5B. This approach⁸ enabled us to mimic the condition of spontaneous arrhythmia generation in our engineered laminar hiPSC-based cardiac microphysiological systems. The reentry circuits generated in this way were stable and had a faster CL ($0.40 \pm 0.03 \text{ s}$) as compared with WT cultures (Figure S5C, $p = 0.02$). This difference may suggest that the instability of the Ca^{2+} store, potentially exacerbated by β -adrenergic stimulation, contributes to shaping the properties of reentrant circuits.

Even in this context, the application of the light stimulation protocol in Ziapin2-loaded cultures achieved a remarkable 100% success rate in terminating the reentry (Figures 4B and 4D, $N = 8$, $p = 0.0002$ with the Fisher exact test), and re-excitability was consistently preserved after each light-induced termination (Figure S4). Within the stepwise stimulation protocol, pulsed light stimulation at 1 Hz terminated reentry in 5 of 8 diseased platforms (Figure 4C).

Insights into the mechanism by which Ziapin2 modulates reentrant arrhythmias

The proposed strategy demonstrated efficacy in optoterminating spiral wave reentry in all experimental cases, highlighting its potential as an antiarrhythmic approach. However, limitations in the experimental setup prevented direct monitoring of the circuit's behavior during optical stimulation, leaving the precise mechanism of optotermination unresolved. In this section, we explore potential mechanisms underlying reentry interruption, focusing on spiral wave drift, conduction block, and filling of the excitable gap as plausible contributors.

Focal illumination, either continuous or patterned, may induce spiral wave drift under specific conditions, such as the presence of a directional gradient in tissue properties.^{12,38} However, for the spiral wave to be terminated by drifting toward an unexcitable boundary, sustained modifications in excitability or refractoriness would be required, which were not achieved under our experimental conditions.^{39,40} As a result, the core of the spiral wave remained stable, preventing it from drifting toward the unexcitable boundary necessary for termination.

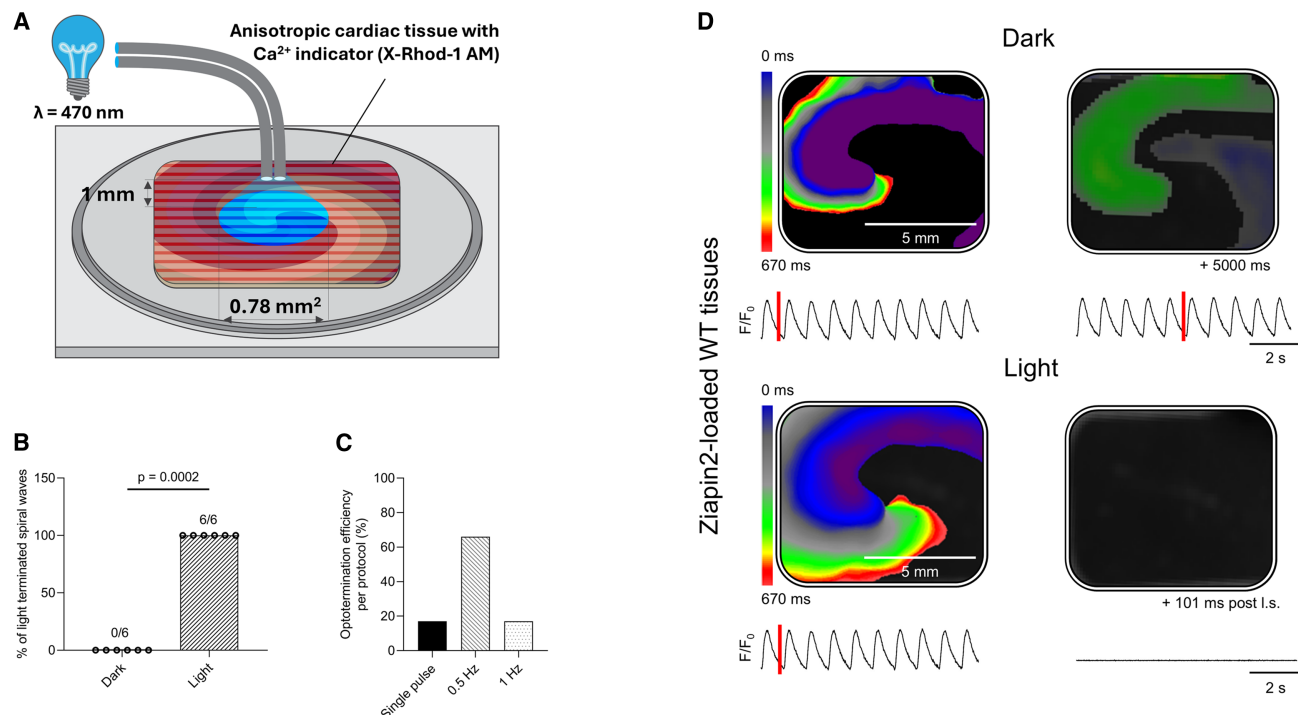


Figure 3. Ziapin2 photoisomerization terminates reentrant circuits induced by S1S2 protocol in WT cultures

(A) Diagram illustrating the setup for optostimulation of Ziapin2-loaded tissues using visible cyan light at a power of 17 mW/mm^2 . Reentry was induced via an electrical S1S2 protocol.

(B) Percentage of successfully terminated reentrant arrhythmias in WT Ziapin2-loaded tissues following the application of light stimulation. Ziapin2 successfully terminated reentrant activity in 6 out of 6 WT tissues tested ($n = 6$ tissues from 3 WT-Cas9 hiPSC-CMs differentiations), $p = 0.0002$, Fisher's exact test).

(C) Percentage of successfully terminated reentrant arrhythmias in WT Ziapin2-loaded tissues following the application of either a single light pulse or pulsed light stimuli at 0.5 Hz and 1 Hz.

(D) Upper panel: WT tissue where the molecule was internalized but not subjected to optical stimulation, showing spiral wave generation and persistence. Bottom panel: The same tissue before and after local illumination. Ziapin2 photoisomerization causes termination of reentry. In both panels, the isochrone map is shown at the top, with the corresponding Ca^{2+} transients acquired at a given time (indicated by the red bar on the traces) below.

Another potential mechanism is conduction block, which occurs when wavefront propagation is halted by regions of refractory tissue.^{9,41} However, this mechanism seems unlikely under the present conditions, as the focal illumination does not provide sufficient spatial coverage nor induce the heterogeneity in excitability required to create a conduction block.^{15,42} Additionally, it was reported that wavefronts propagating through fully excitable tissue remained largely unaffected by the illumination, which was confined to the low-excitability core. Under this condition, rather than being blocked, the spiral wave likely rotates around the illuminated depolarized region, thereby stabilizing itself in the surrounding excitable tissue.³⁹

One plausible mechanism underlying optotermination is the interaction between light-triggered secondary wavefronts and the excitable gap of the reentrant circuit.⁴¹ A light-induced wavefront could collide with and extinguish the spiral wave by filling the critical gap between the head and tail of the reentry.^{43,44} Individual light-induced excitations can perturb the circuit if delivered at a favorable phase, generating wavefronts capable of penetrating the reentrant pathway and promoting its extinction through collision. Consistent with this framework, we observed a trend suggesting that termination efficacy depended on the relationship

between stimulation frequency and reentry CL, with 0.5 Hz appearing more effective in preparations with longer cycle lengths (Figure 3C) and 1 Hz appearing more effective in those with shorter cycle lengths (Figure 4C). This observation may indicate that repeated stimulation increases the probability of phase capture, thereby providing multiple opportunities to interact with the excitable gap. In this scenario, localized illumination at the spiral core may increase the likelihood of a successful interaction, as regions of high curvature are predicted to be more prone to perturbations in excitability and conduction dynamics.⁴⁵ However, while our data clearly demonstrate effective termination, mechanistic conclusions remain speculative. Future studies are needed to validate this hypothesis, including the development of a mathematical model simulating the interaction between Ziapin2 photoisomerization and reentrant arrhythmias, which could offer a valuable quantitative framework for analyzing optotermination dynamics.

Conclusions & future perspectives

We demonstrated effective optotermination of reentrant arrhythmic circuits in engineered human cardiac microtissues by the intramembrane photoswitch Ziapin2. To enable this, we integrated light stimulation, tissue engineering, and hiPSC

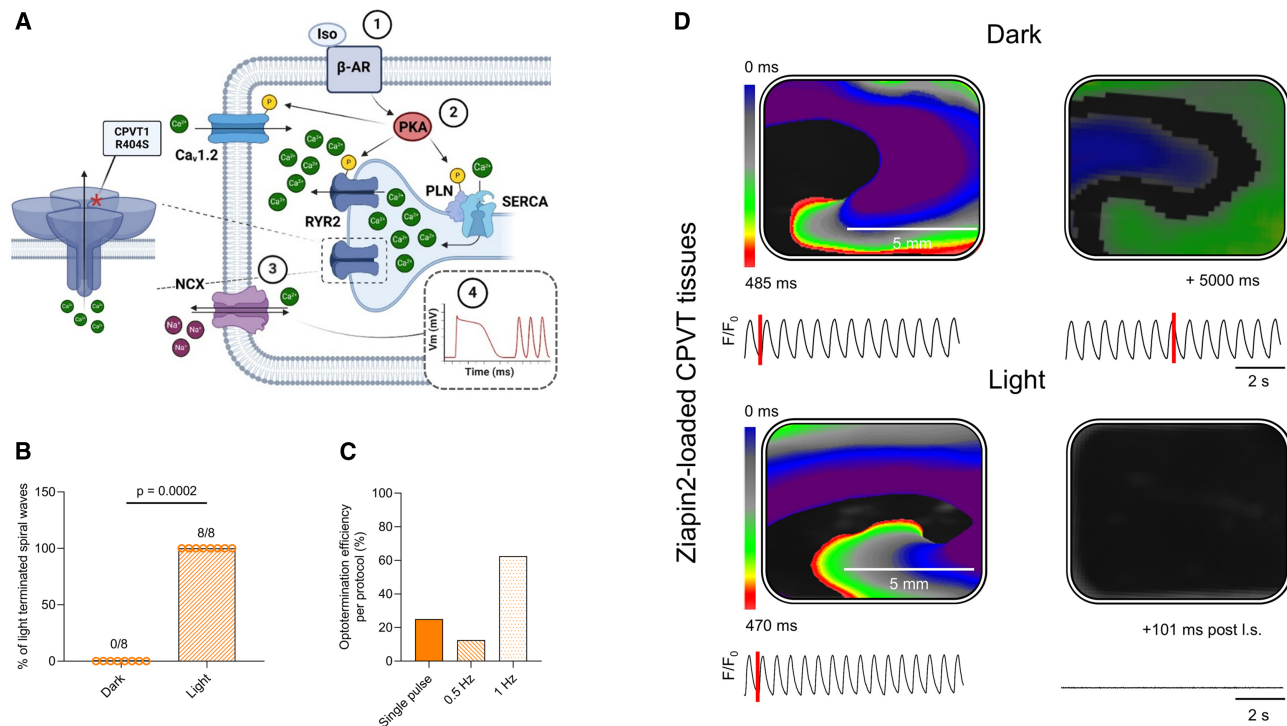


Figure 4. Termination of β -Adrenergic-induced arrhythmias in gene-edited CPVT cultures via Ziapin2-mediated photostimulation

(A) On the left, schematic representation of the RYR2 receptor, highlighting the S404R mutation investigated in this study. On the right, a cartoon illustrating the pathophysiology of CPVT: (1) β -adrenergic stimulation activates the PKA signaling pathway, resulting in the phosphorylation of key Ca^{2+} -handling proteins. (2) This activation increases cytosolic Ca^{2+} levels. (3) The Na^+ - Ca^{2+} exchanger (NCX) functions to extrude Ca^{2+} and import Na^+ , generating a transient inward current. (4) This leads to delayed post-depolarizations that may initiate triggered arrhythmias.

(B) Percentage of successfully terminated reentrant arrhythmias in CPVT Ziapin2-loaded tissues following the application of light stimulation. Ziapin2 successfully terminated reentrant activity in 8 out of 8 CPVT tissues tested ($n = 8$ tissues from 1S404R-gene-edited hiPSC-CMs differentiation, $p = 0.0002$, Fisher's exact test).

(C) Percentage of successfully terminated reentrant arrhythmias in CPVT Ziapin2-loaded tissues following the application of either a single light pulse or pulsed light stimuli at 0.5 Hz and 1 Hz.

(D) Reentry modulation by light in CPVT cultures treated with Ziapin2. In the upper row, Ziapin2-treated cultures exhibit stable and persistent reentry if kept in the dark. In contrast, optical intervention terminates the spiral wave in cultures treated with the molecule and subjected to light stimulation (17 mW/mm^2). In both panels, the isochrome map is shown at the top, with the corresponding Ca^{2+} transients acquired at a given time (indicated by the red bar on the traces) below. Reentry was induced using rapid pacing and β -adrenergic stimulation ($1 \mu\text{M}$ isoproterenol).

technology into a human-based platform for modeling and controlling arrhythmias with high spatiotemporal precision. This was achieved in engineered aligned laminar cardiac microtissues derived from both wild-type and patient-specific gene-edited RYR2-S404R hiPSC-CMs, highlighting the robustness of the approach in an intrinsically arrhythmogenic substrate.

While the exact mechanism of optotermination remains to be fully elucidated, our findings are compatible with a phase-dependent interaction between light-induced excitations and the dynamics of the reentrant circuit, whereby secondary wavefronts may perturb the spiral activity and, under favorable conditions, promote termination through collision. Further studies will be required to directly characterize wavefront dynamics during stimulation and determine the relative contribution of alternative mechanisms. Building on this foundation, the precise spatiotemporal control offered by light opens a broad range of opportunities for developing new antiarrhythmic strategies. For example, subthreshold optical stimulation could be employed to locally modulate electrophysiological properties,^{10,12,13} potentially

reducing energy demands and minimizing off-target effects.²³ In parallel, future efforts will focus on adapting this technology for *in vivo* applications, including the optimization of the absorbance spectrum of phototransducers such as Ziapin2 toward less energetic, more tissue-penetrant wavelengths, determination of optimal dosing, and the development of targeted delivery methods.

In summary, our findings establish a proof of concept for the use of non-genetic, light-responsive small molecules in controlling arrhythmia and support the broader integration of the approach with bioengineered tissue systems as a platform for developing next-generation cardiac therapies.

METHODS

Ethics declaration

No patient-derived materials were used in this study. The hiPSC line used (WTC-Cas9) is commercially available, and the CPVT line was generated by genome editing of the WTC-Cas9 line.

Generation of hiPSC-CMs

hiPSC line WTC-Cas9 was used as a control (Ctrl) in this study. This line was derived using the commercially available control WTC-11 (Coriell Institute; #GM25256) by inserting CAG-rTA::TetO-Cas9 (Addgene #73500)⁴⁶ into the AAVS1 locus to yield a dox-inducible Cas9 hiPSC line. Genome integrity was tested by digital karyotyping (Data not shown). Additionally, cell culture supernatants were routinely screened for mycoplasma contamination using the LookOut® Mycoplasma PCR Detection Kit (Sigma, #MP0035-1KT). To generate the gene-edited hiPSCs carrying the CPVT mutation S404R in the *RYR2* gene, we used the WTC-Cas9 hiPSC line, as reported previously.⁴⁷ hiPSC culture, master cell bank generation, maintenance, cardiac differentiation, cryo-preservation, and cryo-recovery were done as reported previously.³⁴

Tissue chip fabrication

Micromolded gelatin was fabricated on circular acrylic sheets. Paper tape was engraved to create support for gelatin deposition, and gelatin was micromolded as previously reported.^{8,48} Gelatin chips were treated with ultraviolet ozone for 90 s and coated with Geltrex and Fibronectin following an optimized protocol.⁴⁹ After 2 h at room temperature, the coating solution was replaced with PBS. The gelatin chips were stored at 4°C until cell seeding. Thawed iPSC-CMs were plated on gelatin chips and cultured for 5 days after seeding before measurements.

Immunofluorescence imaging

The preparations were fixed for 10 min in 4% paraformaldehyde and 0.25% Triton X-100 in PBS. Non-specific binding sites were blocked by incubating samples with 5% (w/v) bovine serum albumin (BSA) in PBS for 30 min. hiPSC-CMs were stained with Hoechst, Phalloidin 647, and α -actinin conjugate. Samples were mounted on glass slides with ProLong Gold Antifade Mountant, and imaging was performed with an inverted microscope (Olympus IX83, Tokyo, Japan) with an attached spinning disk confocal system (Andor, Concord, MA) using a 20X objective. Cellular orientation was determined using the OrientationJ Measure plugin in the image-processing software (ImageJ).³²

Ziapi2 synthesis and internalization process

Ziapi2 was synthesized as previously described.^{26,28} Micromolar concentrations (50 μ M) of the compound were added to hiPSC-CM cultures directly into the culture medium. Subsequently, the cells were placed in the incubator at 37°C and 5% CO₂. After 7 min, the medium was gently washed out, and the petri dish was rinsed with fresh phenol-red-free RPMI 1640 medium supplemented with B27 minus insulin.

Viability assay

To evaluate Ziapi2 cytotoxicity, an AlamarBlue proliferation assay was performed. For this experiment, hiPSC-CMs were plated one day before the experiment. The samples were incubated with either Ziapi2 or vehicle (DMSO), and light stimulation was applied (1 Hz pulsed light for 1 min) through an optical fiber (cyan, 470 nm). The AlamarBlue Reagent (Invitrogen DAL 1100) was diluted 1:10 in culture medium and incubated for 4 h. The solution without the cell was used as blank. The samples were

transferred to a 96-well plate, and the fluorescence was detected using a plate reader, exciting at 560 nm and measuring the emission at 590 nm.

ROS detection

The fluorogenic CellROX™ Green Reagent (Invitrogen; Carlsbad, CA) was used to assess the oxidative stress induced by optical and electrical stimulation. The experiment included 4 groups of hiPSC-CMs seeded on pre-coated glass coverslips. The first group was subjected to photostimulation for 3 min at 1 Hz, while the second received electrical stimulation at the same frequency. The remaining 2 groups served as controls: a negative control consisting of untreated cells and a positive control of cells treated with 200 μ M menadione for 1 h (Sigma-Aldrich, St. Louis, MO, USA). After stimulation and menadione treatment, the cells were incubated with 5 μ M CellROX™ Green and 20 ng/mL Hoechst stain (ThermoFisher Scientific, Waltham, MA, USA) for 30 min. Following incubation, samples were immediately live-imaged using an EVOS M7000 Imaging System (ThermoFisher Scientific, Waltham, MA, USA). The intensity of CellROX™ Green fluorescence was normalized to the number of Hoechst-positive cells and corrected for background fluorescence.

Optical mapping

To ensure the formation of uniformly anisotropic microtissues, particular attention was paid to avoiding anatomical discontinuities resulting from areas of under-confluence. Prior to recordings, each culture was inspected under the microscope, and only fully confluent preparations were included in the experiments. Any microtissues exhibiting gaps or irregular cell coverage were excluded. After 5 days in culture, microtissues were incubated with the Ca²⁺ indicator X-Rhod-1 AM (2 μ M) in culturing medium for 30 min at 37°C and 5% CO₂. A washout step was performed, the medium was replaced with phenol-red-free RPMI-B27, and the microtissue was mounted on a 37°C heating stage. After staining with the Ca²⁺ indicator, microtissues were equilibrated for at least 5 min. Then, a 20-s recording was acquired in the absence of electrical stimulation to check for spontaneous activity. Only quiescent microtissues were selected for further experimentation.

Optical recordings were acquired using a customized tandem-lens macroscope (Scimedia, Costa Mesa, CA) equipped with a high-speed camera (MiCAM Ultima, Scimedia), a Plan APO 0.63 \times objective, and a 200 mW mercury arc lamp (X-Cite exacte, Lumen Dynamics, Canada) for epifluorescence excitation. The following filter set was used for X-Rhod-1 AM imaging: excitation filter 580/14 nm, dichroic mirror 593 nm long-pass, and emission filter 641/75 nm (Semrock, Rochester, NY). Optical calcium signals were acquired with a sampling time of 2.5 ms and a spatial resolution of 160 μ m/pixel over a 16 \times 16 mm field of view. Recording durations ranged from 10 to 20 s. After recording, a 3 \times 3 spatial filter was applied to the image stack to improve the signal-to-noise ratio.

Protocol of arrhythmia induction

Reentrant activity in WT cultures was induced using a previously established protocol.⁴⁸ Microtissues were first conditioned to electrical stimulation at 1 Hz with an S1 orthogonal field

stimulation (4–5 V/cm, 100 ms pulse duration) for 180 s to ensure stable, uniform propagation across the tissue. Stimulation was applied via two parallel platinum wire electrodes (2 cm long and 2.5 cm apart), positioned along the short axis of the microtissue (Figure S3). Subsequently, a single S2 point stimulus (10 V, 100 ms duration) was delivered via a bipolar platinum electrode spaced 2 mm apart, positioned approximately 1 mm above the microtissue center. The S2 stimulus was applied 200–300 ms after the last S1 stimulus. If no response was observed, the S1–S2 coupling interval was increased iteratively by 10 ms steps; if S2 induced an action potential that propagated through the tissue, the interval was decreased in 5 ms steps. In CPVT cultures, reentrant activity was induced under β -adrenergic stimulation combined with high-frequency pacing. Specifically, cultures were perfused with isoproterenol (1 μ M) and subjected to field stimulation at progressively increasing frequencies (up to 2 Hz). Reentry was considered successfully induced if it persisted through multiple rotations and classified as sustained if it remained detectable for ≥ 30 s.³⁵

Light stimulation

To interrupt reentrant activity, the optical mapping system was adapted for the photostimulation of Ziapin2-loaded microtissues. For point-light stimulation, a focused LED light source (465/25 nm, Doric Lenses) was coupled to an optical fiber positioned at the center of the microtissue ~ 1 mm above the surface, providing a circular spot of 0.78 mm² with an intensity of 17 mW/mm². Optical stimulation was delivered using a sequential stepwise protocol. An initial single light pulse (100 ms duration) was first applied. If activity were still present, pulsed illumination was subsequently delivered at 0.5 Hz and then at 1 Hz (pulse duration: 100 ms). Each stimulation condition was applied for 10 s and repeated up to 5 times before escalating to the next protocol. To control the pacing frequency, pulse duration, and timing of optical stimulation, a custom-written program in LabVIEW (National Instruments, Austin, TX) was implemented. These digital signals were delivered to an analog output module (NI 9264, National Instruments), controlling the LED light source as previously described.^{48,50} Identical illumination protocols were applied to vehicle-treated (DMSO) microtissues as controls. Illumination parameters were kept constant across experiments, and the combination of limited irradiance, short pulse duration, and small illuminated area minimizes the likelihood of photothermal effects.

Statistical analysis

Distribution normality was evaluated using the D'Agostino-Pearson normality test. Sample means were compared using either parametric or non-parametric tests, depending on the type of data (continuous or categorical) and the distribution's normality. For multiple-group comparisons, parametric or non-parametric ANOVA with Tukey's post-hoc correction for continuous data or the Kruskal-Wallis test with Dunn's post-hoc correction for categorical data. The comparison of arrhythmic event occurrences pre- and post-optical stimulation was performed using Fisher's exact test. In the figures, data are presented as mean \pm SEM and when statistical significance was reached the actual *p* value for each comparison is reported as an indicator of statistical robustness.

RESOURCE AVAILABILITY

Lead contact

Requests for further information and resources should be directed to and will be fulfilled by the lead contact, Francesco Lodola (francesco.lodola@unimib.it).

Materials availability

The article and its supplemental information file include experimental procedures, and materials are commercially available or can be prepared as described.

Data and code availability

All data supporting the findings of this study are included within the article and its supplemental information.

ACKNOWLEDGMENTS

The authors would like to thank José Félix Rodríguez Matas and Ludovica Cesaroli for fruitful discussions and Michael Rosnach for the illustrations. Figure 4A was created in BioRender, Lodola, F. (2025) <https://BioRender.com/g77c882>. This research was supported by the NCATS Tissue Chips Consortium (UH3 TR003279), the Harvard Materials Research Science and Engineering Center (No. DMR-2011754) to K.K.P., the Italian Ministry of Universities and Research through the PRIN 2022 project (ID 2022-NAZ-0595) to F.L., the PRIN 2020 project (ID 2020XBFE5) to C.B. and G.L., and the Fondo italiano per la Scienza project (ID FIS00001244) to G.L.

AUTHOR CONTRIBUTIONS

Conceptualization, data curation, formal analysis, investigation, methodology, validation, and writing – original draft, C.F.; data curation, investigation, methodology, and writing – review & editing, K.S.; formal analysis, methodology, and writing – review & editing, V.V.; methodology and writing – review & editing, Y.J.; resources, and writing – review & editing, P.M.; resources, writing – review & editing, M.P.; resources, Y.T.; resources, supervision, writing – review & editing, V.J.B.; resources, supervision, writing – review & editing, W.T.P.; resources, supervision, and writing – review & editing, C.B.; funding acquisition, supervision, writing – review & editing, G.L.; conceptualization, writing – review & editing, A.Z.; funding acquisition, supervision, writing – review & editing, K.K.P.; conceptualization, funding acquisition, project administration, supervision, writing – original draft, F.L.

DECLARATION OF INTERESTS

C.B., G.L., and F.L. are inventors of “photochromic compounds” patent no. EP 3802491 (02/07/2020).

SUPPLEMENTAL INFORMATION

Supplemental information can be found online at <https://doi.org/10.1016/j.celbio.2026.100453>.

Received: September 12, 2025

Revised: January 13, 2026

Accepted: April 2, 2026

REFERENCES

1. Jafri, M.S. (2012). Models of Excitation-Contraction Coupling in Cardiac Ventricular Myocytes. *Methods Mol. Biol.* 910, 309–335. https://doi.org/10.1007/978-1-61779-965-5_14.
2. Kingma, J., Simard, C., and Drolet, B. (2023). Overview of Cardiac Arrhythmias and Treatment Strategies. *Pharmaceuticals (Basel)* 16, 844. <https://doi.org/10.3390/ph16060844>.

3. Haegeli, L.M., and Calkins, H. (2014). Catheter ablation of atrial fibrillation: an update. *Eur. Heart J.* 35, 2454–2459. <https://doi.org/10.1093/eurheartj/ehu291>.
4. Carroll, D.L., and Hamilton, G.A. (2005). Quality of life in implanted cardioverter defibrillator recipients: The impact of a device shock. *Heart Lung* 34, 169–178. <https://doi.org/10.1016/j.hrtlng.2004.10.002>.
5. Di Maria, F., Lodola, F., Zucchetti, E., Benfenati, F., and Lanzani, G. (2018). The evolution of artificial light actuators in living systems: from planar to nanostructured interfaces. *Chem. Soc. Rev.* 47, 4757–4780. <https://doi.org/10.1039/C7CS00860K>.
6. Sung, Y.-L., Wang, T.-W., Lin, T.-T., and Lin, S.-F. (2022). Optogenetics in cardiology: methodology and future applications. *Int. J. Arrhythm.* 23, 9. <https://doi.org/10.1186/s42444-022-00060-4>.
7. Joshi, J., Rubart, M., and Zhu, W. (2020). Optogenetics: Background, Methodological Advances and Potential Applications for Cardiovascular Research and Medicine. *Front. Bioeng. Biotechnol.* 7, 466. <https://doi.org/10.3389/fbioe.2019.00466>.
8. Park, S.-J., Zhang, D., Qi, Y., Li, Y., Lee, K.Y., Bezzerides, V.J., Yang, P., Xia, S., Kim, S.L., Liu, X., et al. (2019). Insights Into the Pathogenesis of Catecholaminergic Polymorphic Ventricular Tachycardia From Engineered Human Heart Tissue. *Circulation* 140, 390–404. <https://doi.org/10.1161/CIRCULATIONAHA.119.039711>.
9. Bruegmann, T., Boyle, P.M., Vogt, C.C., Karathanos, T.V., Arevalo, H.J., Fleischmann, B.K., Trayanova, N.A., and Sasse, P. (2016). Optogenetic defibrillation terminates ventricular arrhythmia in mouse hearts and human simulations. *J. Clin. Investig.* 126, 3894–3904. <https://doi.org/10.1172/JCI88950>.
10. Biasci, V., Santini, L., Marchal, G.A., Hussaini, S., Ferrantini, C., Coppini, R., Loew, L.M., Luther, S., Campione, M., Poggesi, C., et al. (2022). Optogenetic manipulation of cardiac electrical dynamics using sub-threshold illumination: dissecting the role of cardiac alternans in terminating rapid rhythms. *Basic Res. Cardiol.* 117, 25. <https://doi.org/10.1007/s00395-022-00933-8>.
11. Funken, M., Malan, D., Sasse, P., and Bruegmann, T. (2019). Optogenetic Hyperpolarization of Cardiomyocytes Terminates Ventricular Arrhythmia. *Front. Physiol.* 10, 498. <https://doi.org/10.3389/fphys.2019.00498>.
12. Hussaini, S., Venkatesan, V., Biasci, V., Romero Sepúlveda, J.M., Quiñonez Uribe, R.A., Sacconi, L., Bub, G., Richter, C., Krinski, V., Parltz, U., et al. (2021). Drift and termination of spiral waves in optogenetically modified cardiac tissue at sub-threshold illumination. *eLife* 10, e59954. <https://doi.org/10.7554/eLife.59954>.
13. Marchal, G.A., Biasci, V., Loew, L.M., Biggeri, A., Campione, M., and Sacconi, L. (2023). Optogenetic manipulation of cardiac repolarization gradients using sub-threshold illumination. *Front. Physiol.* 14, 1167524. <https://doi.org/10.3389/fphys.2023.1167524>.
14. Ördög, B., De Coster, T., Dekker, S.O., Bart, C.I., Zhang, J., Boink, G.J.J., Bax, W.H., Deng, S., den Ouden, B.L., de Vries, A.A.F., et al. (2023). Optoelectronic feedback control of membrane potential for real-time control of action potentials. *Cell Rep. Methods* 3, 100671, Methods 3. <https://doi.org/10.1016/j.crmeth.2023.100671>.
15. Feola, I., Volkers, L., Majumder, R., Teplenin, A., Schali, M.J., Panfilov, A.V., De Vries, A.A.F., and Pijnappels, D.A. (2017). Localized Optogenetic Targeting of Rotors in Atrial Cardiomyocyte Monolayers. *Circ. Arrhythm. Electrophysiol.* 10, e005591. <https://doi.org/10.1161/CIRCEP.117.005591>.
16. Fenno, L., Yizhar, O., and Deisseroth, K. (2011). The Development and Application of Optogenetics. *Annu. Rev. Neurosci.* 34, 389–412. <https://doi.org/10.1146/annurev-neuro-061010-113817>.
17. Gorostiza, P., and Isacoff, E.Y. (2008). Optical Switches for Remote and Noninvasive Control of Cell Signaling. *Science* 322, 395–399. <https://doi.org/10.1126/science.1166022>.
18. Zhang, J., Wang, J., and Tian, H. (2014). Taking orders from light: progress in photochromic bio-materials. *Mater. Horiz.* 1, 169–184. <https://doi.org/10.1039/C3MH00031A>.
19. Magome, N., Kanaporis, G., Moisan, N., Tanaka, K., and Agladze, K. (2011). Photo-Control of Excitation Waves in Cardiomyocyte Tissue Culture. *Tissue Eng. Part A* 17, 2703–2711. <https://doi.org/10.1089/ten.tea.2010.0745>.
20. Frolova, S.R., Gaiko, O., Tsvelaya, V.A., Pimenov, O.Y., and Agladze, K.I. (2016). Photocurrent of Voltage-Gated Ion Channel Activity by Azobenzene Trimethylammonium Bromide in Neonatal Rat Cardiomyocytes. *PLoS One* 11, e0152018. <https://doi.org/10.1371/journal.pone.0152018>.
21. Izquierdo-Serra, M., Bautista-Barrufet, A., Trapero, A., Garrido-Charles, A., Díaz-Tahoces, A., Camarero, N., Pittolo, S., Valbuena, S., Pérez-Jiménez, A., Gay, M., et al. (2016). Optical control of endogenous receptors and cellular excitability using targeted covalent photoswitches. *Nat. Commun.* 7, 12221. <https://doi.org/10.1038/ncomms12221>.
22. Fehrentz, T., Amin, E., Gördt, N., Strasdeit, T., Moussavi-Torshizi, S.E., Leippe, P., Trauner, D., Meyer, C., Frey, N., Sasse, P., et al. (2025). Optical control of cardiac electrophysiology by the photochromic ligand azobupivacaine 2. *Br. J. Pharmacol.* 182, 1125–1142. <https://doi.org/10.1111/bph.17394>.
23. Sesti, V., Magni, A., Moschetta, M., Florindi, C., Pfeffer, M.E., DiFrancesco, M.L., Guizzardi, M., Folpini, G., Sala, L., Ritacca, A.G., et al. (2025). Membrane-targeted push-pull azobenzenes for the optical modulation of membrane potential. *Light Sci. Appl.* 14, 8. <https://doi.org/10.1038/s41377-024-01669-x>.
24. Riefole, F., Matera, C., Garrido-Charles, A., Gomila, A.M.J., Sortino, R., Agnetta, L., Claro, E., Masgrau, R., Holzgrabe, U., Battle, M., et al. (2019). Optical Control of Cardiac Function with a Photoswitchable Muscarinic Agonist. *J. Am. Chem. Soc.* 141, 7628–7636. <https://doi.org/10.1021/jacs.9b03505>.
25. Leistner, A.L., and Pianowski, Z.L. (2022). Smart Photochromic Materials Triggered with Visible Light. *Eur. J. Org. Chem.* 2022, e202101271. <https://doi.org/10.1002/ejoc.202101271>.
26. DiFrancesco, M.L., Lodola, F., Colombo, E., Maragliano, L., Bramini, M., Paternò, G.M., Baldelli, P., Serra, M.D., Lunelli, L., Marchioreto, M., et al. (2020). Neuronal firing modulation by a membrane-targeted photoswitch. *Nat. Nanotechnol.* 15, 296–306. <https://doi.org/10.1038/s41565-019-0632-6>.
27. Paternò, G.M., Colombo, E., Vurro, V., Lodola, F., Cimò, S., Sesti, V., Molotokaite, E., Bramini, M., Ganzer, L., Fazzi, D., et al. (2020). Membrane Environment Enables Ultrafast Isomerization of Amphiphilic Azobenzene. *Adv. Sci. (Weinh)* 7, 1903241. <https://doi.org/10.1002/adv.201903241>.
28. Vurro, V., Bondelli, G., Sesti, V., Lodola, F., Paternò, G.M., Lanzani, G., and Bertarelli, C. (2021). Molecular Design of Amphiphilic Plasma Membrane-Targeted Azobenzenes for Nongenetic Optical Stimulation. *Front. Mater.* 7, 10. <https://doi.org/10.3389/fmats.2020.631567>.
29. Florindi, C., Vurro, V., Moretti, P., Bertarelli, C., Zaza, A., Lanzani, G., and Lodola, F. (2024). Role of stretch-activated channels in light-generated action potentials mediated by an intramembrane molecular photoswitch. *J. Transl. Med.* 22, 1068. <https://doi.org/10.1186/s12967-024-05902-4>.
30. Vurro, V., Federici, B., Ronchi, C., Florindi, C., Sesti, V., Crasto, S., Maniezzi, C., Galli, C., Antognazza, M.R., Bertarelli, C., et al. (2023). Optical modulation of excitation-contraction coupling in human-induced pluripotent stem cell-derived cardiomyocytes. *iScience* 26, 106121. <https://doi.org/10.1016/j.isci.2023.106121>.
31. Cestariolo, L., Florindi, C., Bertarelli, C., Zaza, A., Lanzani, G., Lodola, F., and Rodríguez Matas, J.F. (2025). Cardiac action potential generation mechanisms via an intramembrane photoswitch. A simulation study. *Biophys. J.* 124, 4505–4516. <https://doi.org/10.1016/j.bpj.2025.04.029>.
32. Vurro, V., Shani, K., Ardoña, H.A.M., Zimmerman, J.F., Sesti, V., Lee, K.Y., Jin, Q., Bertarelli, C., Parker, K.K., and Lanzani, G. (2023). Light-triggered cardiac microphysiological model. *APL Bioeng.* 7, 026108. <https://doi.org/10.1063/5.0143409>.
33. Florindi, C., Jang, Y., Shani, K., Moretti, P., Bertarelli, C., Lanzani, G., Parker, K.K., Lodola, F., and Vurro, V. (2025). A Cardiac Microphysiological System

- for Studying Ca²⁺ Propagation via Non-genetic Optical Stimulation. *J. Vis. Exp.* 67823. <https://doi.org/10.3791/67823>.
34. Prondzynski, M., Berkson, P., Trembley, M.A., Tharani, Y., Shani, K., Bortolin, R.H., Sweat, M.E., Mayourian, J., Yucel, D., Cordoves, A.M., et al. (2024). Efficient and reproducible generation of human iPSC-derived cardiomyocytes and cardiac organoids in stirred suspension systems. *Nat. Commun.* 15, 5929. <https://doi.org/10.1038/s41467-024-50224-0>.
35. Iravanian, S., Nabutovsky, Y., Kong, C.-R., Saha, S., Bursac, N., and Tung, L. (2003). Functional reentry in cultured monolayers of neonatal rat cardiac cells. *Am. J. Physiol., Heart Circ. Physiol.* 285, H449–H456. <https://doi.org/10.1152/ajpheart.00896.2002>.
36. Mohamed, U., Napolitano, C., and Priori, S.G. (2007). Molecular and Electrophysiological Bases of Catecholaminergic Polymorphic Ventricular Tachycardia. *J. Cardiovasc. Electrophysiol.* 18, 791–797. <https://doi.org/10.1111/j.1540-8167.2007.00766.x>.
37. Bezzerides, V.J., Caballero, A., Wang, S., Ai, Y., Hyland, R.J., Lu, F., Heims-Waldron, D.A., Chambers, K.D., Zhang, D., Abrams, D.J., et al. (2019). Gene Therapy for Catecholaminergic Polymorphic Ventricular Tachycardia by Inhibition of Ca²⁺/Calmodulin-Dependent Kinase II. *Circulation* 140, 405–419. <https://doi.org/10.1161/CIRCULATIONAHA.118.038514>.
38. Hu, Y., Ding, Q., Wu, Y., Jia, Y., Li, T., Yu, D., and Zhan, X. (2024). Control of spiral waves in myocardial tissue by optogenetics and temperature. *Nonlinear Dyn.* 112, 19421–19439. <https://doi.org/10.1007/s11071-024-10028-9>.
39. Hussaini, S., Lädke, S.L., Schröder-Schetelig, J., Venkatesan, V., Quiñonez Uribe, R.A., Richter, C., Majumder, R., and Luther, S. (2023). Dissolution of spiral wave's core using cardiac optogenetics. *PLoS Comput. Biol.* 19, e1011660. <https://doi.org/10.1371/journal.pcbi.1011660>.
40. Hussaini, S., Mamyraiym Kyzy, A., Schröder-Schetelig, J., Lädke, S.L., Venkatesan, V., Diaz-Maue, L., Quiñonez Uribe, R.A., Richter, C., Bikta-shev, V.N., Majumder, R., et al. (2024). Efficient termination of cardiac arrhythmias using optogenetic resonant feedback pacing. *Chaos* 34, 031103. <https://doi.org/10.1063/5.0191519>.
41. Sasse, P., Funken, M., Beiert, T., and Bruegmann, T. (2019). Optogenetic Termination of Cardiac Arrhythmia: Mechanistic Enlightenment and Therapeutic Application? *Front. Physiol.* 10, 675. <https://doi.org/10.3389/fphys.2019.00675>.
42. Watanabe, M., Feola, I., Majumder, R., Jangsangthong, W., Teplenin, A.S., Ypey, D.L., Schalij, M.J., Zeppenfeld, K., de Vries, A.A.F., and Pijnappels, D.A. (2017). Optogenetic manipulation of anatomical re-entry by light-guided generation of a reversible local conduction block. *Cardiovasc. Res.* 113, 354–366. <https://doi.org/10.1093/cvr/cvx003>.
43. Crocini, C., Ferrantini, C., Coppini, R., Scardigli, M., Yan, P., Loew, L.M., Smith, G., Cerbai, E., Poggesi, C., Pavone, F.S., et al. (2016). Optogenetics design of mechanistically-based stimulation patterns for cardiac defibrillation. *Sci. Rep.* 6, 35628. <https://doi.org/10.1038/srep35628>.
44. Karathanos, T.V., Bayer, J.D., Wang, D., Boyle, P.M., and Trayanova, N.A. (2016). Opsin spectral sensitivity determines the effectiveness of optogenetic termination of ventricular fibrillation in the human heart: a simulation study. *J. Physiol.* 594, 6879–6891. <https://doi.org/10.1113/JP271739>.
45. Tomii, N., Yamazaki, M., Arafune, T., Kamiya, K., Nakazawa, K., Honjo, H., Shibata, N., and Sakuma, I. (2018). Interaction of phase singularities on the spiral wave tail: reconsideration of capturing the excitable gap. *Am. J. Physiol., Heart Circ. Physiol.* 315, H318–H326. <https://doi.org/10.1152/ajpheart.00558.2017>.
46. Mandegar, M.A., Huebsch, N., Frolov, E.B., Shin, E., Truong, A., Olvera, M.P., Chan, A.H., Miyaoka, Y., Holmes, K., Spencer, C.I., et al. (2016). CRISPR Interference Efficiently Induces Specific and Reversible Gene Silencing in Human iPSCs. *Cell Stem Cell* 18, 541–553. <https://doi.org/10.1016/j.stem.2016.01.022>.
47. Wang, G., Yang, L., Grishin, D., Rios, X., Ye, L.Y., Hu, Y., Li, K., Zhang, D., Church, G.M., and Pu, W.T. (2017). Efficient, footprint-free human iPSC genome editing by consolidation of Cas9/CRISPR and piggyBac technologies. *Nat. Protoc.* 12, 88–103. <https://doi.org/10.1038/nprot.2016.152>.
48. Lee, K.Y., Park, S.-J., Matthews, D.G., Kim, S.L., Marquez, C.A., Zimmerman, J.F., Ardoña, H.A.M., Kleber, A.G., Lauder, G.V., and Parker, K.K. (2022). An autonomously swimming biohybrid fish designed with human cardiac biophysics. *Science* 375, 639–647. <https://doi.org/10.1126/science.abh0474>.
49. Kim, S.L., Trembley, M.A., Lee, K.Y., Choi, S., MacQueen, L.A., Zimmerman, J.F., De Wit, L.H.C., Shani, K., Henze, D.E., Drennan, D.J., et al. (2023). Spatiotemporal cell junction assembly in human iPSC-CM models of arrhythmogenic cardiomyopathy. *Stem Cell Rep.* 18, 1811–1826. <https://doi.org/10.1016/j.stemcr.2023.07.005>.
50. Park, S.-J., Gazzola, M., Park, K.S., Park, S., Di Santo, V., Blevins, E.L., Lind, J.U., Campbell, P.H., Dauth, S., Capulli, A.K., et al. (2016). Phototactic guidance of a tissue-engineered soft-robotic ray. *Science* 353, 158–162. <https://doi.org/10.1126/science.aaf4292>.

Supplemental information

**Optotermination of spiral wave reentry
by a membrane-targeted phototransducer**

Chiara Florindi, Kevin Shani, Vito Vurro, Yongjun Jang, Paola Moretti, Maksymilian Prondzynski, Yashasvi Tharani, Vassilios J. Bezzerides, William T. Pu, Chiara Bertarelli, Guglielmo Lanzani, Antonio Zaza, Kevin Kit Parker, and Francesco Lodola

Supplementary Information

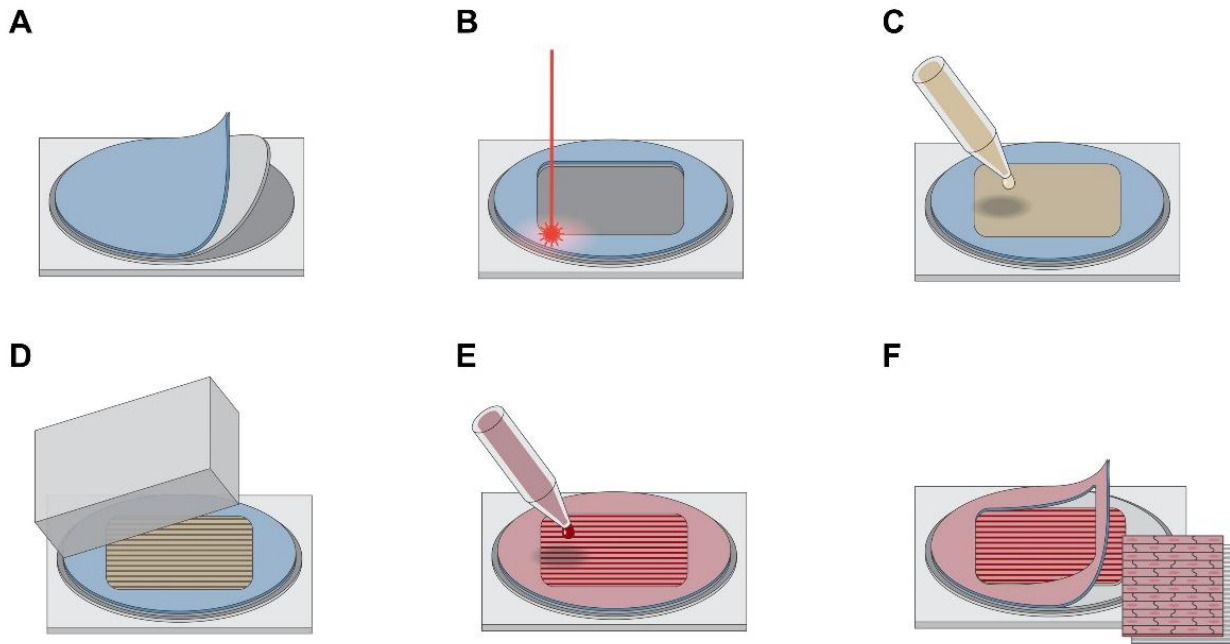


Figure S1: Diagram of the laminar cardiac tissue preparation process. **A.** The process begins with the placement of two overlapping layers of paper tape onto an acetate base. **B.** Both paper layers are then patterned using laser ablation to define the desired geometry. **C.** A gelatin solution is applied onto the patterned substrate, covering the exposed areas. **D.** The gelatin layer is shaped and cured using a PDMS stamp featuring a linear pattern, which helps define the tissue architecture. **E.** Once the gelatin structure is in place, cardiac cells are seeded onto the prepared surface. **F.** Finally, the top layer of paper tape is removed, revealing the final geometry of the engineered tissue (see inset).

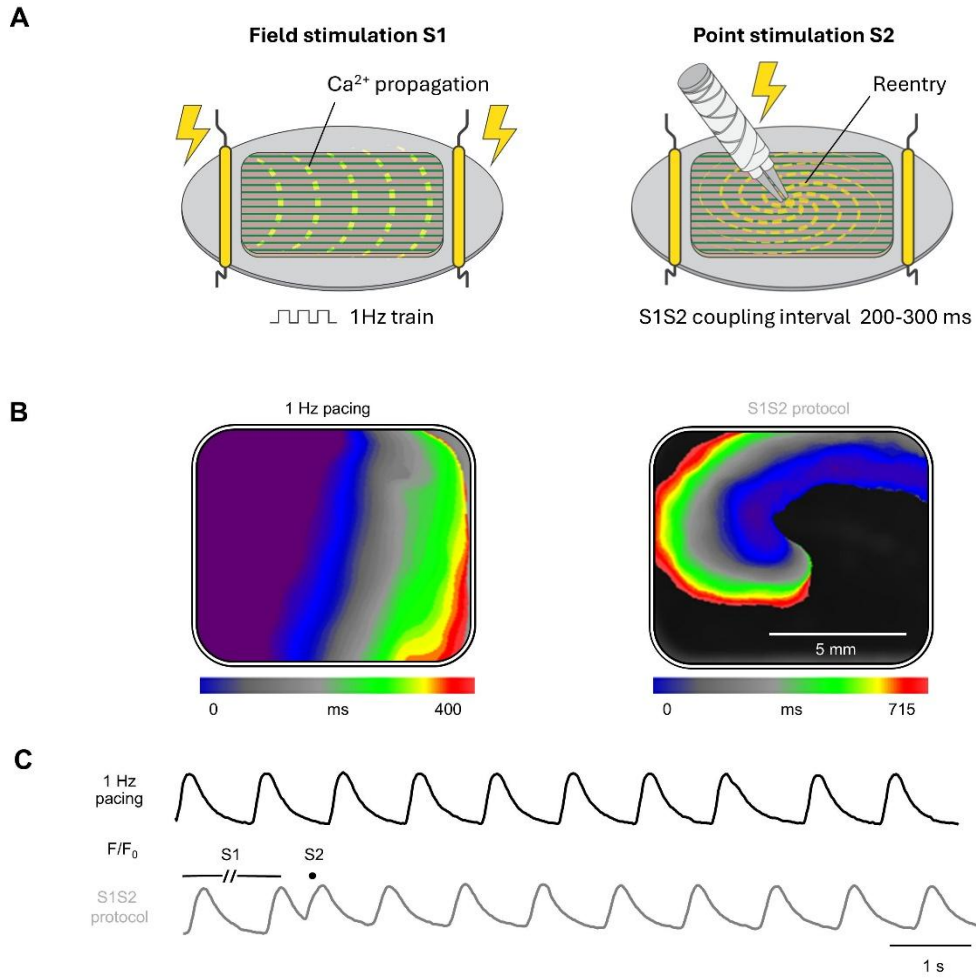


Figure S2: Induction of reentrant activity in WT tissues using the S1S2 Protocol. **A.** Schematic representation of the electrode configuration used for S1S2 stimulation and induction of reentrant activity in anisotropic cardiac tissue (see methods for details). **B.** Representative isochrone maps displaying the reentrant activity induced at the center of the platform after applying the S1S2 arrhythmia induction protocol. **C.** Representative Ca²⁺ traces recorded in WT tissues, showing the transition from regular pacing to arrhythmic activity initiated by the S1S2 protocol.

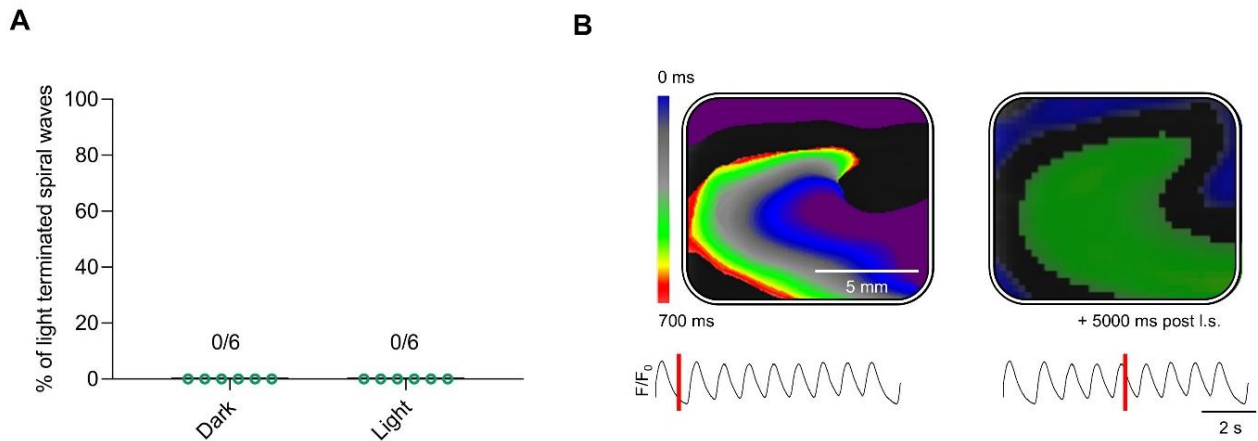


Figure S3: Vehicle-treated tissues maintain persistent reentry after optical stimulation. A. DMSO-loaded cultures failed to terminate reentrant activity in all 6 tissues from 3 WT-Cas9 hiPSC-CMs differentiations. Statistical analysis was performed using the Fisher's exact test ($p = 1$). **B.** The figure shows the isochrone maps at the top, with the corresponding Ca^{2+} transients acquired at a given time (indicated by the red bar on the traces) below from WT tissues treated with vehicle (DMSO) and subjected to the same optical stimulation protocol used for Ziapin2-incubated tissues. Reentry was induced via an electrical S1S2 protocol.

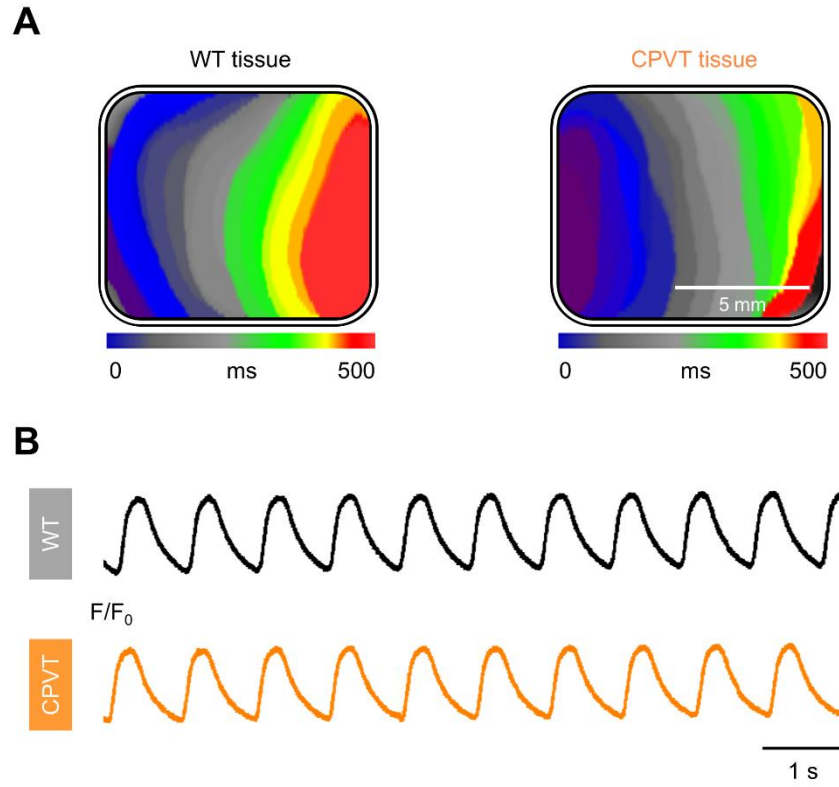


Figure S4: Preserved tissue excitability following optotermiation. Isochrone maps illustrating activation patterns (**A**) and corresponding Ca^{2+} transients (**B**) recorded in WT (black) and CPVT (orange) engineered tissues during 1 Hz field electrical stimulation after optical termination of reentrant arrhythmias.

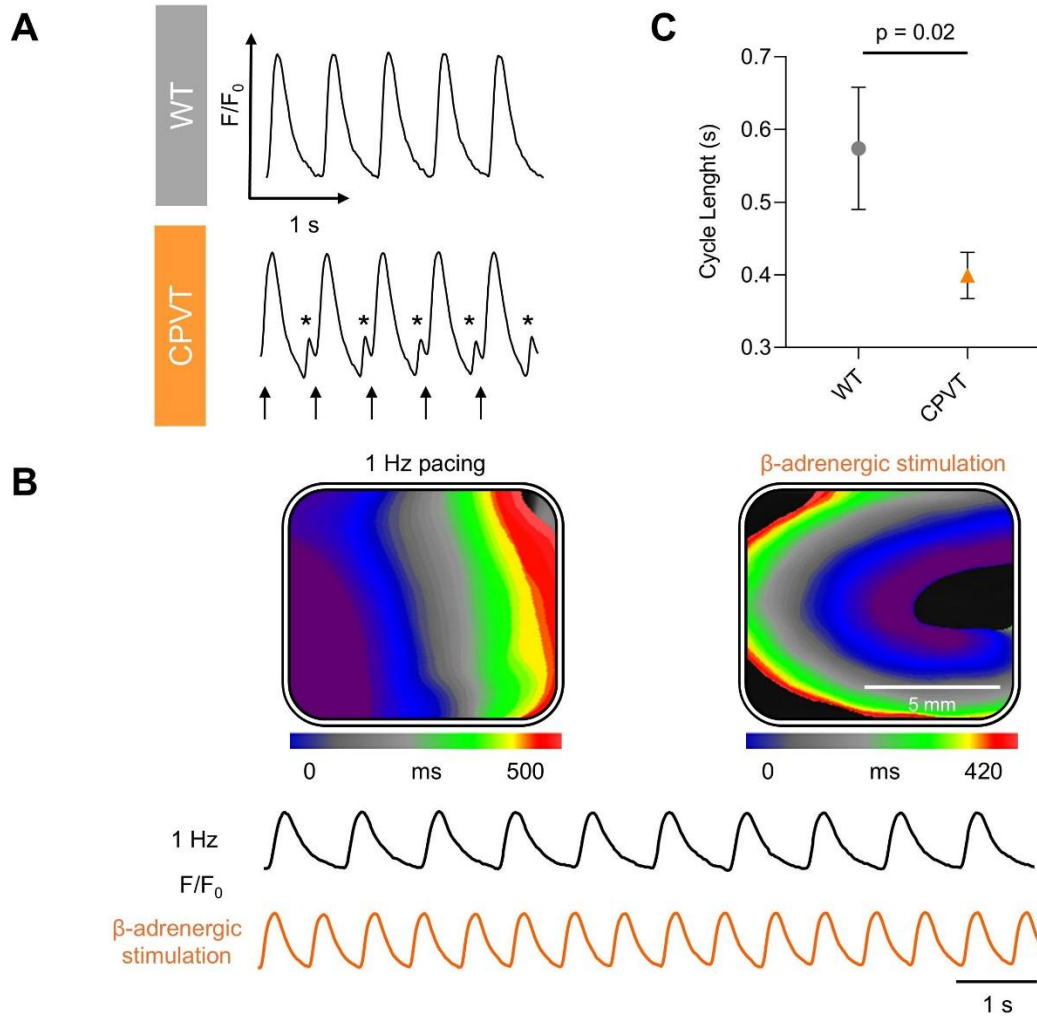


Figure S5: Phenotypic assessment and reentrant activity in CPVT Ziapin2-loaded tissues. A. Representative Ca^{2+} transients for WT and CPVT tissues. Asterisks indicate spontaneous Ca^{2+} release events (i.e. uncontrolled, untriggered releases of Ca^{2+} from the sarcoplasmic reticulum into the cytosol of cardiomyocytes, occurring independently of normal excitation-contraction coupling), and the upward arrow marks electrical stimulation. **B.** Representative isochrone maps (top) and relative Ca^{2+} traces (bottom) displaying the reentrant activity in response to rapid pacing (> 2 Hz) and $1 \mu\text{M}$ isoproterenol, showing the transition from regular pacing to arrhythmic activity initiated by β -adrenergic stimulation. **C.** Cycle length of reentry in WT ($N = 6$ tissues from 3 differentiations) and CPVT ($N = 8$ tissues from 1 differentiation) hiPSC-CMs tissues. Data are represented as mean \pm SEM. Statistical analysis was performed using the Mann–Whitney test.